Materials Advances

ROYAL SOCIETY OF CHEMISTRY

PAPER

View Article Online
View Journal | View Issue

Check for updates

Cite this: *Mater. Adv.*, 2022, 3, 7328

Toxic metal–organic gels using a unique pyridine–pyrazole based ligand with Pb(II), Cd(II) and Hg(II) salts: multi-stimuli responsiveness and toxic dye adsorption†

Manasi Roy, * Amit Adhikary, Sayan Saha and Raju Mondal *

Received 29th April 2022,
Accepted 13th July 2022

DOI: 10.1039/d2ma00483f

rsc.li/materials-advances

The present work reports the design and synthesis of a low molecular weight gelator (LMWG), namely 1-(3-(pyridin-2-yl)-1*H*-pyrazole-5-carboylimino)ethyl)phenyl)ethylidene)-3-(pyridin-2-yl)-1*H*-pyrazole-5-carbohydrazide (**H_3BPDP**). **H_3BPDP** acts as a gelator to encapsulate the toxic heavy metal ions Pb(II), Cd(II) and Hg(II) and forms metal-organic gels (MOGs). Microscopic analyses such as SEM and TEM of the MOGs revealed intertwining fibrous networks for Cd and Hg, whereas interesting nanoscale metal-organic particles (NMOPs) were formed with Pb-MOG. After heating the Pb-MOG for a few hours and keeping the solution for slow evaporation for a few days, remarkably single crystals were grown. Single-crystal X-ray analysis indeed confirmed the encapsulation of Pb^{2+} by the gelator, **H_3BPDP**, and a two-dimensional coordination polymer of composition $[Pb_5(BPDP)_2(NO_3)_4(DMF)]_n$ was observed. Moreover, EDAX analysis also confirmed the encapsulation of Pb, Cd, and Hg elements from their respective xerogels. The formation of MOGs with the toxic metals was also monitored by ^{1}H NMR titration and ligand participation in the formation of the metal–N bond was clearly perceptible by monitoring the N–H proton. The MOGs exhibited sol–gel transformation by applying thermo-, chemical, pH- and mechano-stimuli. Besides that, the xerogels of the Cd-based MOG and Pb-based MOG have shown remarkable efficiency (>80%) to adsorb the toxic methyl orange (MO) dye, which may be utilized in wastewater treatment.

Introduction

For the last few decades, metal organic gels (MOGs) formed by low molecular weight organic gelators (LMWGs) have been an interesting area[1–5] because of their extensive applications in drug delivery,[6,7] chemosensing,[8,9] catalysis,[10,11] wastewater treatment,[12–15] *etc.* Various non covalent interactions, *e.g.* π–π interaction, hydrophobic interaction, and H-bonding interactions are responsible for the self-assembly of LMWGs to make a cross-linked network of gel matrix.[16,17] Compared to organo-gels resulting from purely the self-assembly of LMWGs, MOGs or metallogels are a relatively less explored research field.[18–20] The use of metals in metallogel imparts extra stability by forming strong coordination bonds and consequently increases the thermal stability and porous nature of the structural assembly.[21–23] Current research has been focused on the development of metallogels based on metal ligand strong coordination bonds and metal ions in MOGs can show unique properties such as magnetism, conductance, catalysis,[24] fluorescence,[25] sensing, toxic dye removal, *etc.*[26–29]

Solvent selectivity can greatly influence the self-assembly of a gel matrix (Scheme 1) as well as the crystal structure of metal organic frameworks or coordination polymers.[30,31] A gel can be acquired by the systematic balance of crystallization and dissolution of the gelator.[32–34] Recently it has been well established that N-moiety containing gelators are a great choice for better gelation.[35–37] So inspired from that we have designed and synthesized a novel pyridine–pyrazole moiety containing Schiff-base ligand to explore its potential for the formation of metallogels with toxic heavy metals, *e.g.* Pb(MOG **1**), Cd (MOG **2**), Hg (MOG **3**), *etc.* These toxic metals are non-biodegradable and have an adverse effect in our human body.[38,39] Keeping this in mind, this ligand was chosen as it contains quite a large number of N-atoms for better coordination with these toxic metals as well as four –NH groups for assembling molecules through H-bonding.

With the above context, we report herein the gelation properties of ligands with toxic metals as well as the formation

School of Chemical Sciences, Indian Association for the Cultivation of Science, 2A &2B, Raja S. C. Mullick Road, Kolkata 700032, West Bengal, India.
E-mail: manasiroy88@gmail.com, icrm@iacs.res.in

† Electronic supplementary information (ESI) available: Synthesis of the ligand, TGA, PXRD analysis of all MOGs and MOF **1**, effect of pH on the MOGs and crystallographic data file of MOF **1**. CCDC 2058105. For ESI and crystallographic data in CIF or other electronic format see DOI: **https://doi.org/10.1039/d2ma00483f**

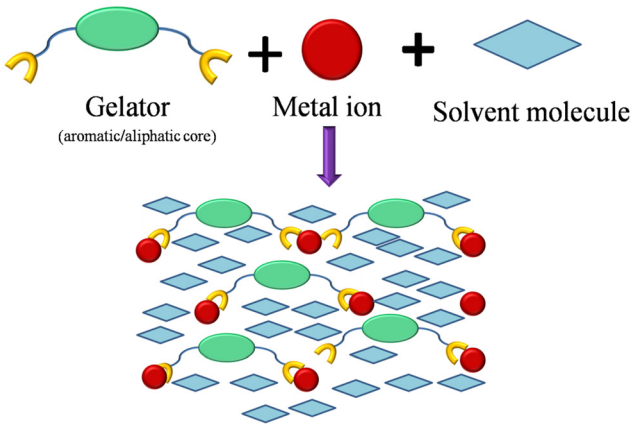

Scheme 1 General schematic representation of the formation of the metallogel.

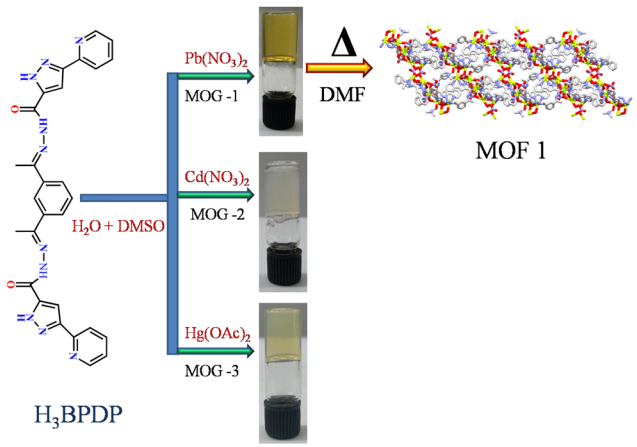

Scheme 2 Schematic representation of the synthesis of MOGs **1–3** and MOF **1**.

of one novel MOF with Pb^{2+} (Scheme 2) ions. In excellent agreement with our synthetic object, the formation of Pb-MOF itself is a challenging task in a large, multidentate ligand system. Structural analysis has shown that MOF **1**$[Pb_5(BPDP)_2(NO_3)_4(DMF)]_n$ is formed with SBU containing multinuclear metal centers. For the present case, the toxic heavy metal based MOGs have shown also remarkable capability to adsorb the toxic dye methyl orange. Moreover, the MOGs exhibit an interesting reversible sol–gel transformation in response to multi-stimuli (like chemical-, pH-, thermo-, and mechano-induced).

Results and discussion

Microscopic study

Morphological studies of all the MOGs have been performed by using various types of microscopic techniques to get some visual insight. Not only the morphological study but also the formation of nanoparticles has been investigated by scanning electron microscopy (SEM) and transmission electron microscopy (TEM). For MOG **1**, a gel was prepared using 2 equivalents of metal salt and the TEM image shows the aggregation of

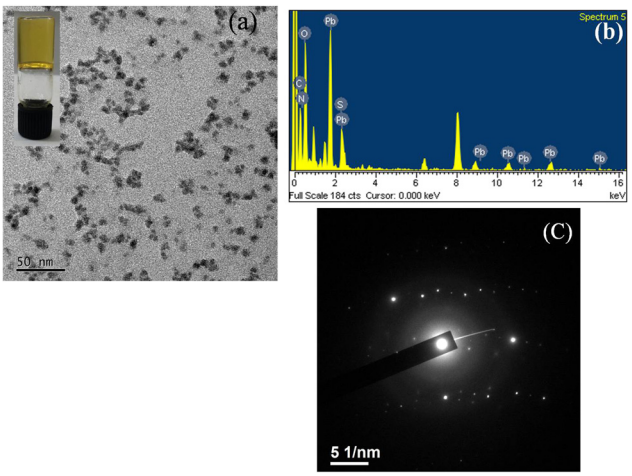

Fig. 1 (a) TEM images of freshly prepared MOG **1** showing NMOPs formation; (b) EDAX and (c) SAED of MOG **1**.

numerous round shaped NMOPs (nanoscale metal–organic particles) with an approximate size of 8–10 nm (Fig. 1a). To further confirm the formation of nanoparticles, energy dispersive X-ray analysis (EDAX) was performed on these NMOPs, which shows the presence of Pb, C, N, O and S elements (Fig. 1b) and this result ruled out the possibility of the formation of only lead nanoparticles. Selected-area electron diffraction (SAED) was also performed on these NMOPs and revealed the crystalline nature of the individual particles (Fig. 1c). The crystallinity of MOG **1** is further supported by the PXRD pattern of the dried gel of lead nitrate ligand **H_3BPDP** (Fig. S2, ESI†).

Morphological studies of MOG **2** and MOG **3** showed more interesting and unique features. The TEM image of MOG **2** revealed cross-linked, intertwined, infinite length fibrous network with 8–10 nm average diameter (Fig. 2a). A time resolved study revealed an interesting morphological transformation from fibers to almost square shaped particles when the gel

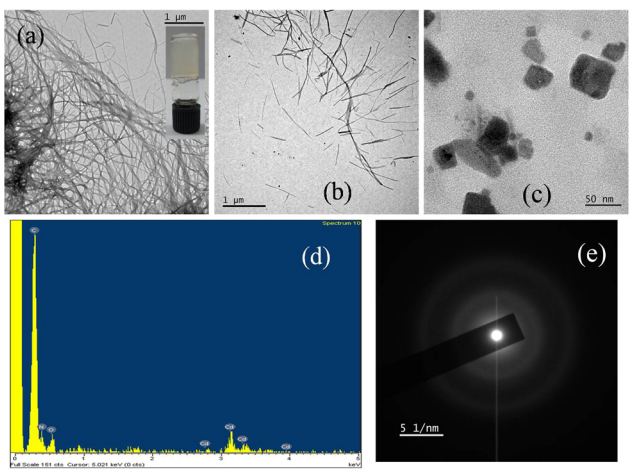

Fig. 2 (a) TEM images of freshly prepared MOG **2**; (b) gradual NMOPs formation of MOG **2**; (c) nano-scale metal organic particles of Cd-compound; (d) EDAX and (e) SAED of MOG **2**.

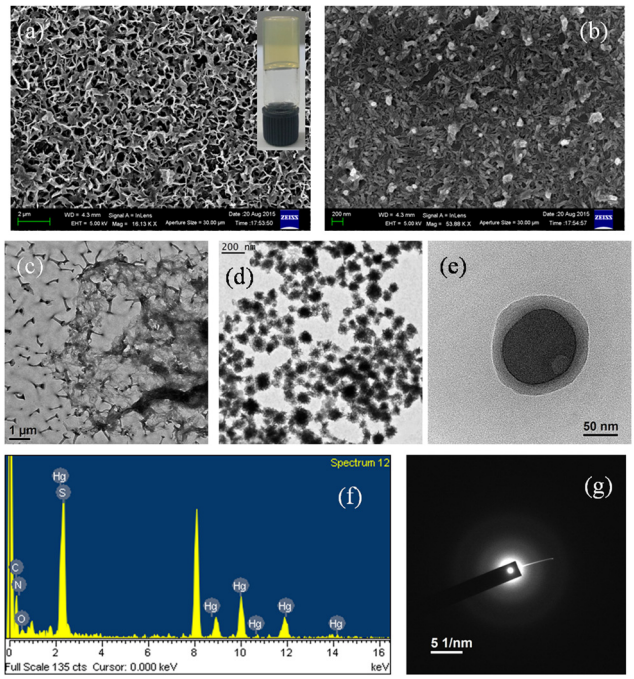

Fig. 3 SEM images of (a) freshly prepared MOG **3** and (b) after 3 weeks; (c–e) TEM images of MOG **3** showing gradual NMOPs formation; (f) EDAX and (g) SAED of MOG **3**.

was kept for one week. This is due to the formation of a metal–ligand complex which appeared as nanoscale metal–organic particles (Fig. 2b). The number as well as size of the particles increased as evident from the TEM images (Fig. 2c). Square-shaped particles of diameter ranging from 10–40 nm were visible in the micrographs when the same sample was kept for one month. The EDAX result (Fig. 2d) showed that these nano-particles were made up of Cd, N, C and O. SAED was conducted on these particles (Fig. 2e) and it exhibited the non-crystalline nature of the particles, which was further confirmed by the PXRD data (Fig. S2, ESI†).

A similar interesting transformation from fibres to spherical particles was observed for MOG **3** from the SEM and TEM micrographs (Fig. 3a–e). The size of the round shaped particles was ranging from 40–90 nm. EDAX analysis clearly revealed the presence of Hg, C, N, O, and S (Fig. 3f); hence these particles can be regarded as nano metal organic particles (NMOPs). SAED study (Fig. 3g) on these particles showed the non-crystalline nature of each particle and that was well supported by the PXRD pattern of a dried gel of mercury acetate and ligand **H_3BPDP** (Fig. S2, ESI†).

Rheological Studies of the MOGs

The strength of all the MOGs was investigated by strain sweep rheology (Fig. 4a–c). All the rheology measurements were performed with gels made from 1 wt% ligand concentration. In the strain sweep experiment, the elastic modulus (G') and viscous modulus (G'') were measured as a function of increasing strain amplitude from 0.01 to 100% at 10 radian per s^{-1} constant angular frequency. From this experiment, it is observed that for all the gel samples the elastic modulus (G') is higher than the viscous modulus (G''), indicating the true gel-like nature of the material. From this study, it is observed that all the gel materials are stable up to 10% shear strain. After that, MOG **2** breaks down at 12.8% and MOG **3** breaks at 23.7% strain. The Pb gel transforms into a sol at 62.5% strain, which is quite high enough indicating the strong nature of the gel material due to the formation of strong coordination bonds with the metal ion.[40] Thixotropic results also showed the stronger nature of the Pb gel in comparison to the other gel materials (Fig. 4d–f).

Spectral studies

NMR titration. In order to explore the metal-ligand coordination, ^{1}H NMR titration was performed using DMSO-d_6 as s solvent. Furthermore, to monitor the change of mainly the N–H proton (amide N–H and pyrazole N–H) and whether it has participated in complex formation or in H-bond formation, NMR titration was done for individual MOGs. Firstly, for the pure ligand, the spectroscopic studies were performed taking 4 mg ligand in 0.45 ml DMSO-d_6 (red line). Then for MOG **1**, 10 microlitre of lead nitrate solution (made by 200 mg in 0.2 ml DMSO-d_6) was added each time. A clear change of N–H proton was observed after certain steps of the experiment. Firstly, broadening with slight downfield shift and then disappearance of the N–H proton indicate the participation of the proton in H-bonding and complex formation, respectively, of the ligand with Pb-metal ions as a pyrazolate form (Fig. 5a). For MOG **2** and MOG **3**, ^{1}H NMR titration was performed in a similar way, but for both the gels we could not perform the experiment until the end due to the formation of an opaque solution. From Fig. 5b, it is clearly revealed that for the Cd gel, only broadening of the signal occurred. This can be attributed to the extensive H-bonding in the gel state, but no coordination bond between the metal and ligand primarily. Furthermore, these results corroborate with the TEM images taken at one month intervals. For the Hg gel, the common trends of downfield shift and broadening of the signal for the N–H proton were observed (Fig. 5c), which again confirms the formation of a coordination bond with the metal ion and the participation of the proton in hydrogen bond formation between the molecules and with the solvent molecules. For all the MOGs, slight downfield shifting with broadened signals of the aromatic protons indicates the π-stacking of the aromatic ring in the gel state.

FT-IR spectra. In order to get further insights into the supramolecular interactions *e.g.* π–π stacking between the gelator molecules, and participation of diamide and the N–H moiety of the pyrazole group in the self-assembling gelation process, FT-IR spectral studies have been performed for the free ligand and individual MOGs in the dried state. The xerogels exhibited a distinct change from the free ligand. The free ligand exhibits a strong adsorption peak at 3440 cm^{-1}, which is attributed to the pyrazole N–H stretching frequency (Fig. 6a). This peak appeared for the xerogels at the lower frequency side with slight broadening; *e.g.* 3426 cm^{-1} for MOG **1**, 3437 cm^{-1} for MOG **2**; and 3435 cm^{-1} for MOG **3**. Similarly the peaks at 1680 cm^{-1} and 1532 cm^{-1} were assigned to the C=O stretching frequency and N–H bending frequency, respectively, for the free

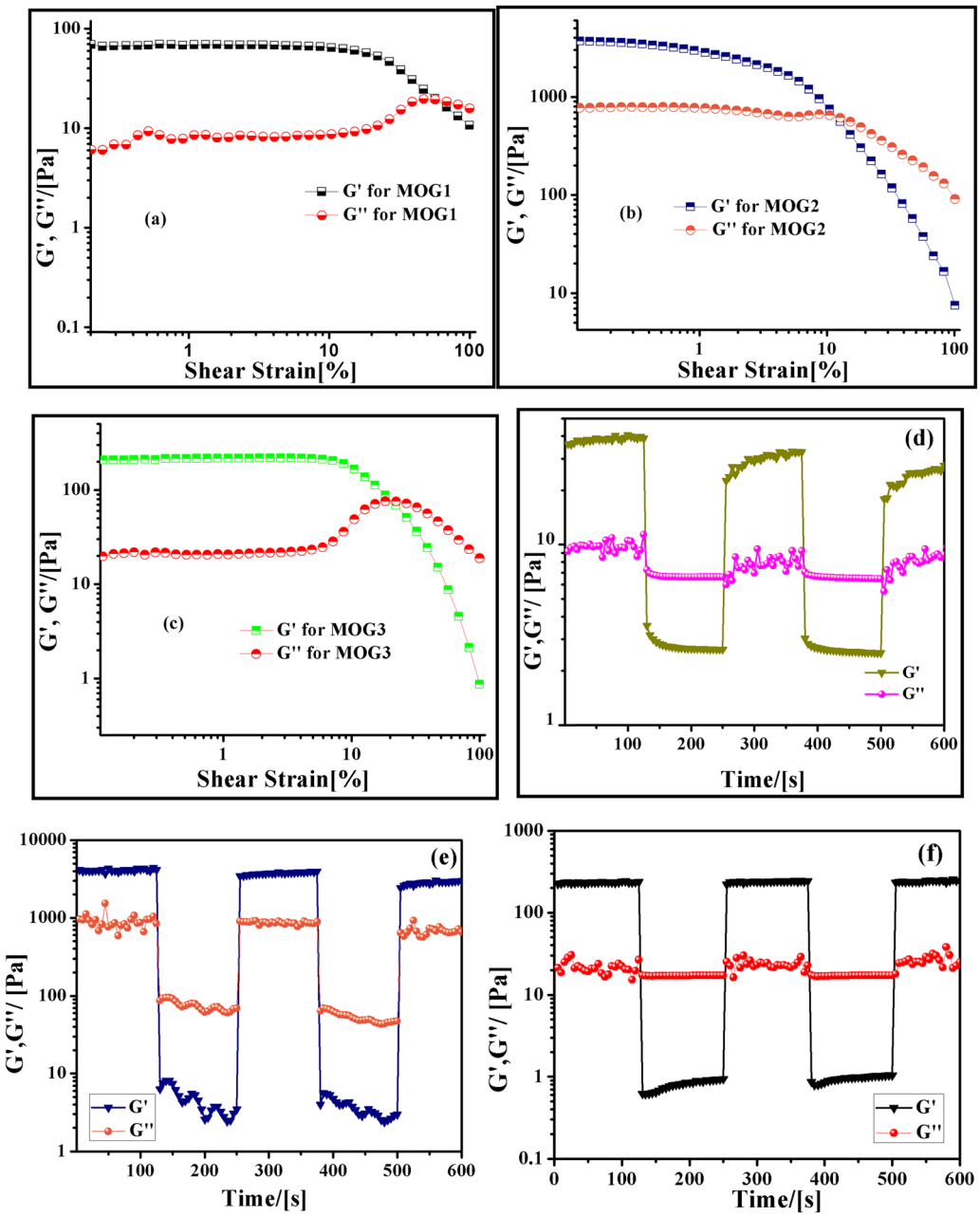

Fig. 4 Plots of elastic modulus (G') and viscous modulus (G'') of MOG **1**, MOG **2**, and MOG **3** as a function of (a–c) shear strain; thixotropic behavior of (d) MOG **1**, (e) MOG **2** and (f) MOG **3**.

ligand. The corresponding peaks were shifted to 1644 cm^{-1} and 1541 cm^{-1} for Pb, 1619 cm^{-1} and 1525 cm^{-1} for Cd, and 1671 cm^{-1} and 1526 cm^{-1} for the Hg xerogel. The decrease in N–H and C=O frequency clearly indicates the participation in intermolecular H-bonding in the gel state (Fig. 6b–d).

Multi-stimuli responsive MOGs

Reversible transformation of the gel[41–43] material to the liquid form (sol) has been investigated with a variety of stimuli,[44,45] like mechano-, thermo-, chemical- and pH-induction for MOGs **1–3** (Fig. 7a–c). All MOGs turned out to be temperature sensitive. So, we studied the effect of temperature by heating and cooling the MOGs and as a result, a reversible sol-gel transformation was noticed (Fig. 10). We also studied the chemical responsiveness of the MOGs by using a very well known metal chelating agent, namely ethylene diamine tetra acetic acid (EDTA), to capture the metal ion from the gel matrix. The same equivalent of solid EDTA was added on the top of the gel surface as that of the metal salt in the gel. The solution was kept undisturbed for a few days and in the case of MOG **2** and MOG **3** penetration of the solid EDTA was negligibly small (Fig. 7b and c), whereas for MOG **1** containing Pb(II) ions, the solid EDTA showed better penetration signifying easier complex formation. Subsequently, MOG **1** transforms into a transparent solution, while a white precipitate

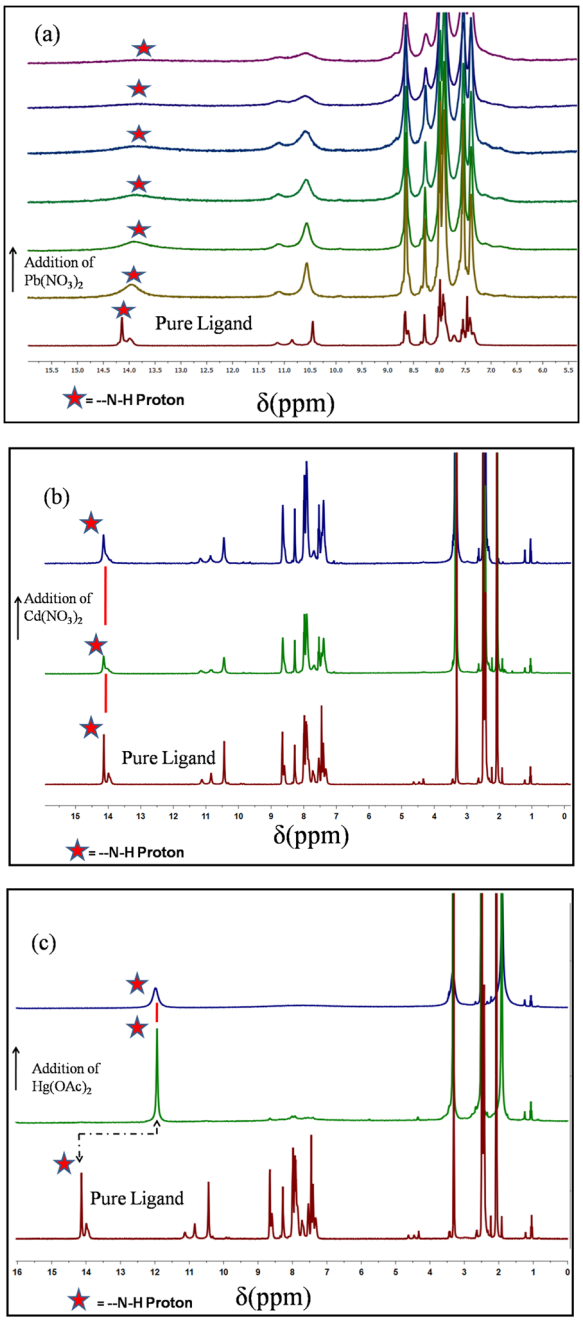

Fig. 5 NMR titration of (a) MOG **1**, (b) MOG **2** and (c) MOG **3**.

deposited at the bottom of the vial. Further investigation reveals that the white precipitate contains Pb(II) and EDTA, and the clear solution contains the remaining ligand. To further confirm whether the clear solution contains ligand or not, we added lead nitrate salt to it again and the solution turned into a gel (MOG **1**) as before. So, from this result we can conclude that the Pb(II) ion might form a stable complex with EDTA at a faster rate than the other MOGs.

Beside the thermo, mechano and chemoresponsive natures, the MOGs were detected to be pH sensitive (Fig. S5, ESI†) and they were stable in the pH range of 6–8. The pH responsiveness of these MOGs was examined using 0.2 M hydrochloric acid (pH below 6) and the equivalent amount of NaOH (0.2 M) as the experimental acid-base pair. Upon addition of 0.2 M HCl, the MOGs were converted into a clear solution and upon addition of an equivalent amount of NaOH solution, the gel was restored. This reversible sol-gel transformation can be explained by breaking and making new bonds between the metal and the ligand molecules.[46]

Dye adsorption studies

The textile, pharmaceutical, food, cosmetics, and paper industries utilize mostly reactive, mutagenic organic toxic dyes, which are very much responsible for water pollution. For the last two decades, several smart efficient materials like MOFs with high surface area, clay and supramolecular gels have been considered as a potent dye adsorbing agent in the literature.[47–50] A major aspect for a dye adsorbing agent is that it should have two parts for efficient dye adsorption: (i) the presence of a hydrophilic part to interact with water through H-bonding, and (ii) the presence of a hydrophobic part to adsorb the organic dye.[51,52] Interestingly, our ligand system possesses both of these key features. The presence of amide groups in our ligand makes it more efficient for dye removal *via* hydrogen bonding interaction with the dye molecules. For this purpose, time dependent UV-Vis spectroscopy was performed to determine the rate of adsorption of methyl orange dye by the MOGs. As a result, a 10^{-5} molar aqueous solution of methyl orange (MO) was prepared for the dye adsorption study. In a typical reaction, 4 mg of xerogel was allowed to soak in 3 mL of MO dye stock solution and kept undisturbed. After a few hours, the resulting solution was almost completely decolorized in the presence of Pb and Cd xerogel, but no remarkable change was observed for the Hg xerogel (Fig. 8). The color change process was monitored by time dependent UV-Vis spectra of the MO solution containing the respective xerogel with the characteristic absorption maxima of the dye at 464 nm (Fig. 9). Over time, the intensity of the peak showed a steady decrease with continuous bleaching of the orange colour of the dye and it reached equilibrium within 7–8 hours. The rate of the reaction follows pseudo-first-order kinetics,[50] and can be written as:

$$\ln(C_t/C_0) = \ln(A_t/A_0) = -K_{app}t$$

where C_t = concentration of dye at time "t" and C_0 = concentration of dye at $t = 0$, A_t = absorbance of dye at time t and A_0 = absorbance of dye at $t = 0$, and K_{app} = apparent rate constant.

From the equation $(C_0 - C_t/C_0) \times 100\%$ we can calculate the adsorption efficiency of the respective MOG. This result showed us that within 7–8 hours, the Pb xerogel adsorbs 80.5% of the dye solution and the Cd xerogel adsorbs 82.5% of the dye solution (Fig. 10). So both the xerogels are considered as a suitable candidate for toxic dye removal by efficient dye adsorption into their gel matrix.

Reusability of the MOGs. The organic azo dye methyl orange (MO) can exist in both its anionic and cationic form depending on the pH of the solution. Previously we have studied the effect of pH on the MOGs or xerogels. Finally, the reusability of these dye adsorbed xerogels was investigated. For that, the dye adsorbed xerogel was washed with an equivalent amount of

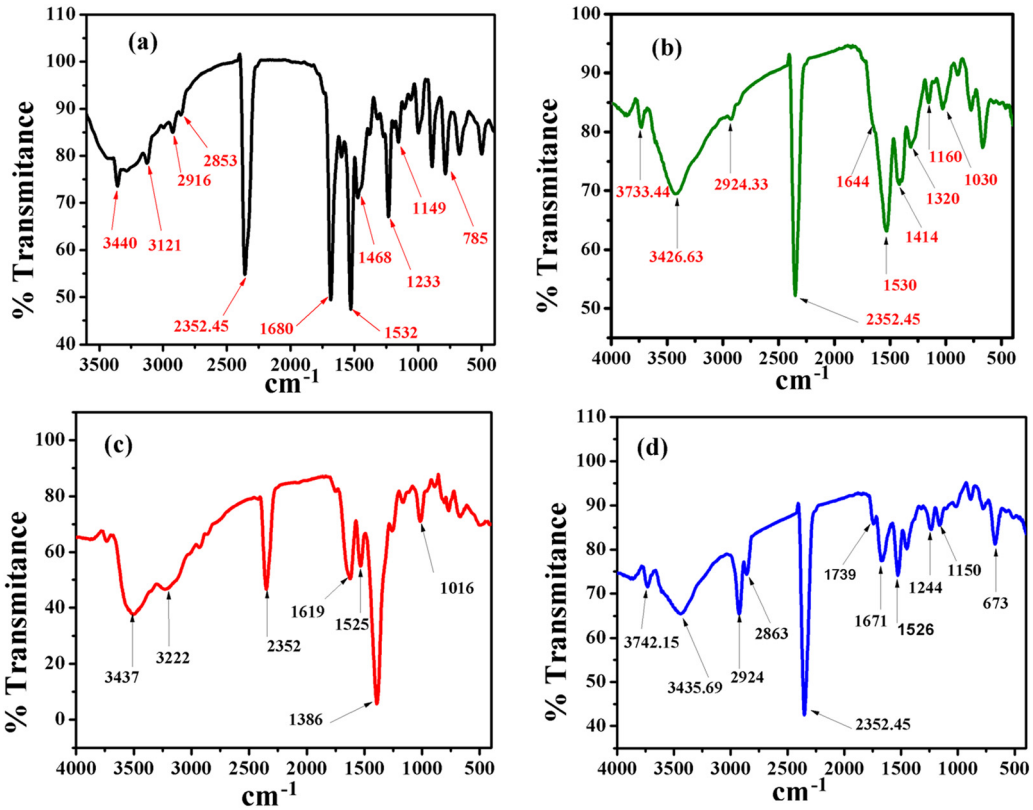

Fig. 6 FT-IR spectra of (a) the ligand, (b) the MOG **1** Xerogel, (c) the MOG **2** xerogel and (d) the MOG **3** xerogel.

0.2 M HCl and 0.2 M NaOH solution followed by distilled water. Then, the dye-free xerogel was equally capable of adsorbing a new set of MO dye, indicating the electrostatic interactions that facilitate adsorption/removal of the dye molecules. The reusability of the MOGs was confirmed by the PXRD patterns of the xerogels of MOG **1** and MOG **2**. It is satisfactorily shown that before and after dye adsorption, the PXRD patterns remain the same for both of the MOGs (Fig. S3, ESI†). In continuation of our interest, we showed that the free ligand **H_3BPDP** itself was unable to adsorb the toxic dye, which suggests that electrostatic interaction was not the only key factor, but that the metal-ligand polymeric network also plays a pivotal role to adsorb toxic dye molecules through its gel-matrix.

Crystal structure elucidation for MOF 1

Single crystal X-ray analysis reveals that MOF **1** crystallizes in the triclinic $P\bar{1}$ space group. The phase purity of MOF **1** was confirmed by PXRD analysis (Fig. S4 in ESI†) where the experimental PXRD patterns satisfactorily matched with the simulated pattern. The asymmetric unit of MOF**1** consists of five Pb^{2+} ions, two trianionic ligand moieties along with four NO_3^- anions and lattice solvent molecules (Fig. 11a). Each ligand does not coordinate symmetrically with the metal centers. The ligand exhibits asymmetric binding where the enol-oxygen has μ-bridging (C–O distance = 1.27(3) Å) at one side, whereas on the other side the keto-oxygen does not have any bridging (C–O distance = 1.21(3) Å). Hence, overall, the ligand is asymmetric having three deprotonated hydrogen centers. The structural arrangement of MOF **1** exhibits a rare and interesting two dimensional network in which the metal ions seem to have a helical character. In this structure, there are two types of structural building units (SBUs) (Fig. 11b and c), which combine to construct MOF **1**.

A closer structural investigation reveals that the central Pb^{2+} is eight coordinated having N_4O_4 coordination. Two oxygens of each nitrate as well as four nitrogen atoms of two pyrazoles and two pyridyl moieties coordinate to the Pb^{2+} metal to fulfill the coordination. Interestingly, the coordination environment of each Pb center is not the same and the coordination number significantly varies from five-coordinated to octa-coordinated as seen from Fig. 12. Consequently, the geometry around the metal centers is changed according to the coordination numbers. Polyhedra are connected through edge sharing and corner sharing.

Experimental section

All reagents except for the ligand were purchased from available commercial sources and were used without further purification.

Instrumentation

FT-IR. FT-IR spectra were recorded on a Nicolet MAGNA-IR 750 spectrometer with samples prepared as KBr pellets.

X-Ray crystallography. X-ray diffraction intensities for MOF 1 were collected at 100 K on a Bruker D8 Venture APEX-3, using Mo-K_α radiation with a CMOS detector. The structure was

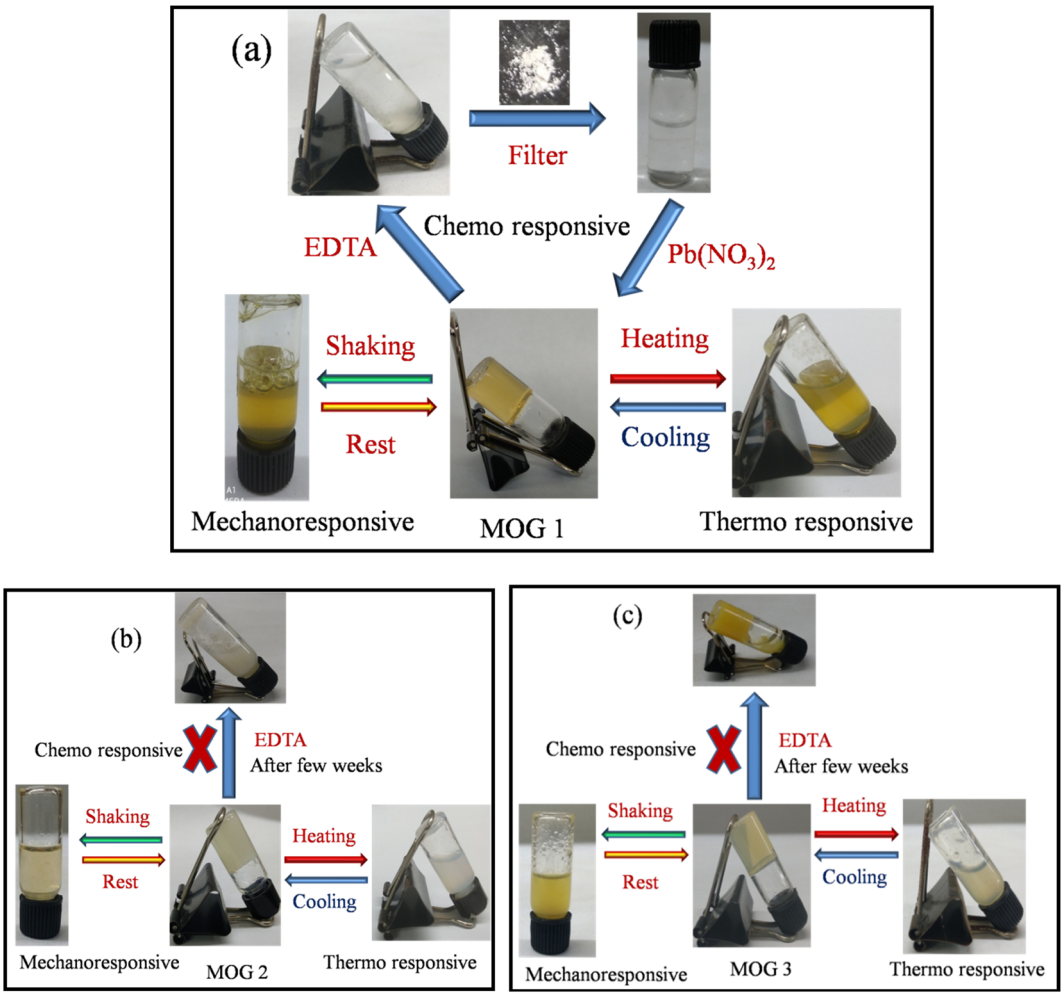

Fig. 7 Illustration of the reversible gel–sol transformation of (a) MOG **1**, (b) MOG **2** and (c) MOG **3** by a variety of stimuli (mechano-, thermo-, and chemical-stimuli).

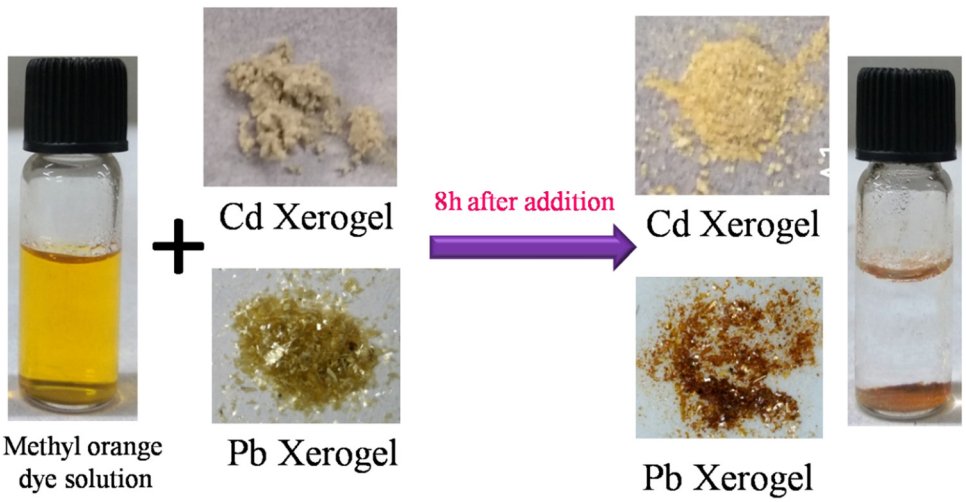

Fig. 8 Illustration of dye adsorption by the xerogels of MOG-**1** & MOG-**2**; noticeable colour change of a methyl orange dye solution for the xerogels after 8 hr due to adsorption of the dye by the xerogel.

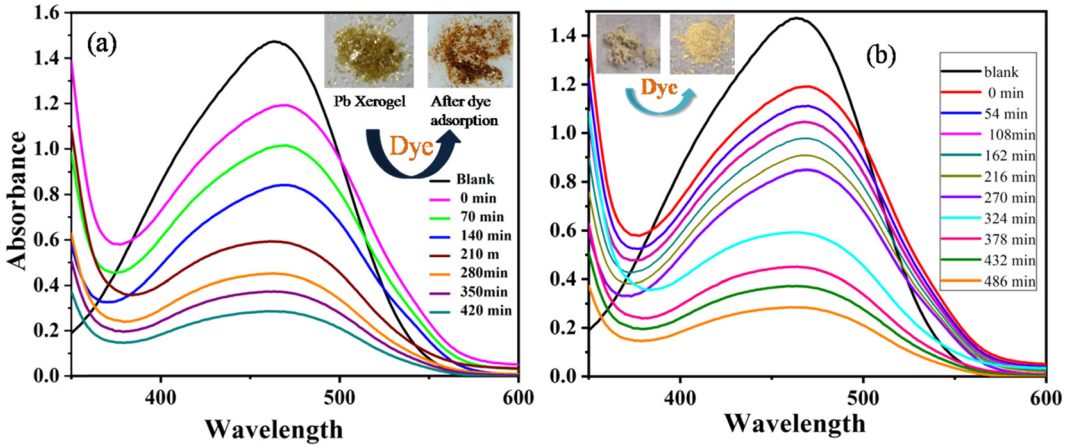

Fig. 9 Time dependent UV-vis absorption spectra of a methyl orange dye solution (black line) after the addition of (a) MOG **1** xerogel & (b) MOG **2** xerogel (colored lines).

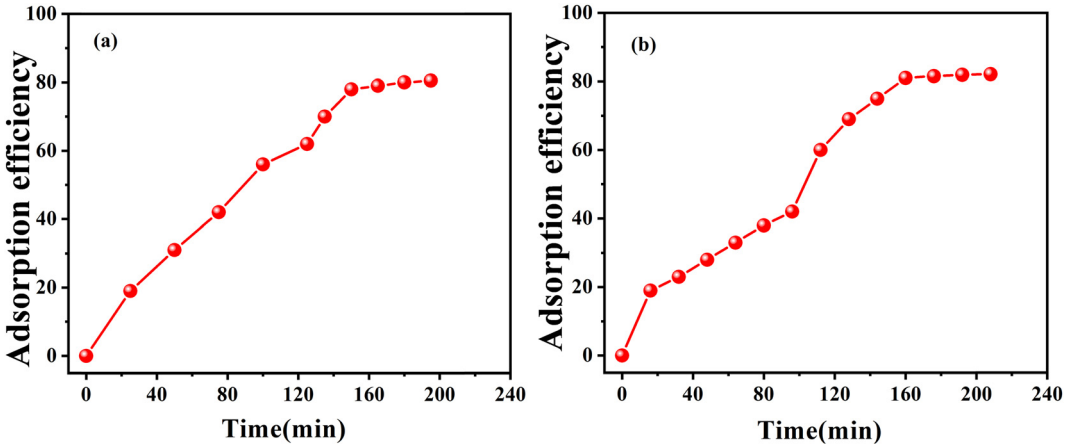

Fig. 10 Adsorption efficiency of dried (a) MOG **1** and (b) MOG **2** in methyl orange dye solution.

solved by direct methods in SHELXS and refined by full matrix least-squares on F^2 in SHELXL.[53] The CCDC number is 2058105.† Crystallographic data and refinement parameters for MOF **1** are given in a tabular form (Table S1, ESI†). Bond distances and bond angles of MOF **1** are summarized in Table S2 (ESI†).

Microscopic studies

SEM (scanning electron microscopy). A very small amount of freshly prepared gel sample was taken in 1 ml of DMSO solvent and sonicated continuously for 24 hours, then placed on a clean glass slide and then dried by slow evaporation. The material was then allowed to dry under vacuum at 35 °C for 50 hours. The materials were silver-coated, and the micrographs were taken in FESEM apparatus Jeol Scanning Microscope-JSM-6700F and Carl Zeiss AG SUPRA 55 VP-41-32.

TEM (transmission electron microscopy). Freshly prepared small amounts of gel sample were taken in 1 ml DMSO solvent, and the sample was sonicated for a few hours. Then, 1 drop of this solution was drop cast on a 300 mesh carbon-coated copper grid, and it was mounted on a Jeol JEM 2010 HRTEM for TEM imaging.

Thermo gravimetric (TGA) analysis. To check the thermal stability of all the reported MOGs, thermo gravimetric analysis was performed (Fig. S1 in ESI†) in the presence of a N_2 atmosphere with a heating rate of 10 °C min^{-1} in a platinum crucible using TA Instruments SDT Q600.

X-Ray powder diffraction. PXRD analysis for the reported metallogels and MOF1 (Bruker AXS D8 Advance Powder ($CuK\alpha_1$ radiation, λ = 1.5406 Å) X-ray diffractometer) was carried out to check the phase purity of the samples (Fig. S2 in ESI†). All the samples were scanned in the range of 2θ = 0–50° with the scan rate was 1 s per step.

Spectral studies. Time dependent UV-visible absorption spectra of the dye solution containing the respective xerogel were recorded at ambient temperature on a Cary-500 UV-Vis Spectrophotometer. For each experiment in the dye adsorption study, 4 mg of xerogel was added to 3 mL of stock dye aqueous solution (10^{-5} M) prepared by dissolving 3 mg of methyl orange dye in 100 mL distilled water.

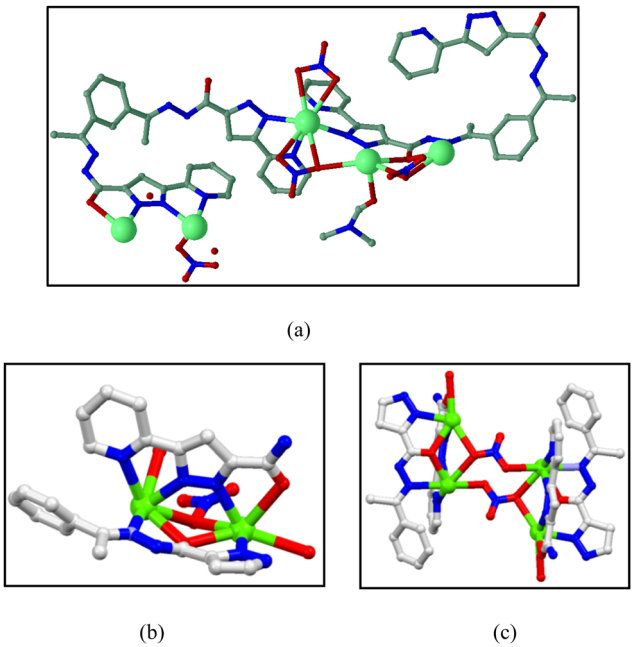

Fig. 11 (a) Asymmetric unit of MOF **1**. (b) Representative unit of MOF **1** (SBU I) and (c) SBU II resulting from the combination of two SBU I.

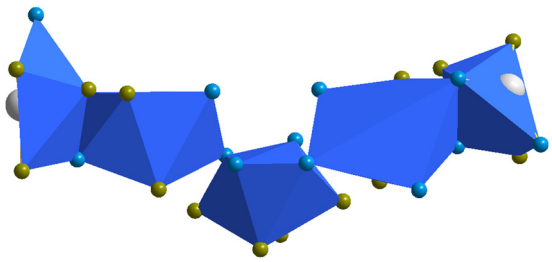

Fig. 12 Polyhedral representation of MOF **1**. Other atoms are omitted for clarity.

Rheology experiment. The strength of all the MOGs was investigated using strain sweep and stress sweep and thixotropic measurement using an Anton Paar MCR 102 Rheometer with a 25 mm diameter parallel plate and constant tool gap of 300 μm. A gel sample was taken in a 5 mL vial and transferred onto the Peltier plate. All measurements were carried out at 25 °C. The stress sweep study was performed with a stress ramp from 0.1 to 200 Pa at an angular frequency of 6.284 rad s^{-1}.

Synthetic aspect

Ligand **H_3BPDP** is insoluble in water and methanol and fairly soluble in DMSO and DMF. In general, for typical gel formation, a DMSO solution of the ligand was mixed with an aqueous solution of the heavy metal salt.

Synthesis of ligand. The synthetic procedure of ligand **H_3BPDP** (Scheme S1, ESI†) was described in the supporting file.

Synthesis of metallogels (MOGs)

Synthesis of MOG 1. 10 mg ligand (1 wt%) was taken in 0.3 ml of DMSO solvent, and then the ligand solution was mixed with 0.7 ml aqueous solution of $Pb(NO_3)_2$ with continuous shaking. An instantly viscous yellow colour solution was formed, which was then sonicated for 50 min and after that a clear yellow gel was formed.

Synthesis of MOG 2. 10 mg ligand (1 wt%) was taken in 0.5 ml of DMSO solvent. Then the ligand solution was mixed with 0.5 ml aqueous solution of $Cd(NO_3)_2$ with continuous shaking. The clear solution was sonicated for 35 min and after that an opaque white colour gel was formed.

Synthesis of MOG 3. 10 mg ligand (1 wt%) was taken in 0.5 ml of DMSO solvent, and then the ligand solution was mixed with 0.5 ml aqueous solution of $Hg(OAc)_2$ dropwise with continuous shaking. A viscous light yellow colour solution was formed. Then it was sonicated for 40 min and after that a clear light yellow gel was formed.

Synthesis of MOF 1. When MOG **1** was heated, the gel was converted to sol form. Then, 2 ml DMF solvent was added to the solution (for better chelation). After heating the solution with continuous stirring for 2 h, the solution was allowed to cool down to room temperature. Afterwards the solution was kept for slow evaporation for a few days. Then light yellow colored, small, square-shaped crystals were grown from the solution. The crystals were filtered and washed with methanol and then kept in dry air (42% yield).

Conclusion

In conclusion, we have explored the gel properties of a pyridine-pyrazole containing Schiff-base ligand in the presence of toxic heavy metal ions like Pb(II), Cd(II) and Hg(II). We have also successfully synthesized an SBU-based 2D Pb-MOF. Based on several experiments, it has been demonstrated that coordination to metals, hydrophobic interaction, hydrogen bonding, π–π stacking, and van der Waals interactions play a significant role in promoting the self-assembly of the supramolecular gel. Rheological studies revealed high mechanical strength of these MOGs. Reversible gel–sol transformations in response to thermo-, mechano-, pH and chemical-stimuli were also exhibited by these MOGs. Moreover, these supramolecular MOGs exhibited significant toxic dye adsorption into their gel matrix, so the reported MOGs may be considered as potential materials for waste-water treatment.

Conflicts of interest

There are no conflicts to declare.

Acknowledgements

R. M. gratefully acknowledges the Department of Science and Technology (DST), India, for financial assistance (DST/INT/SWD/VR/P-05/2019). M. R. is thankful to the Indian Association for the Cultivation of Science (IACS) for the research fellowship. The authors thank Mr Krishna Sundar Das (School of Chemical

Sciences, IACS) for his assistance in the rheological data collection.

References

1 X. Yu, L. Chen, M. Zhang and T. Yi, Low-molecular-mass gels responding to ultrasound and mechanical stress: towards self-healing materials, *Chem. Soc. Rev.*, 2014, **43**, 5346–5371.
2 N. Roy, B. Bruchmann and J.-M. Lehn, DYNAMERS: dynamic polymers as self-healing materials, *Chem. Soc. Rev.*, 2015, **44**, 3786–3807.
3 N. M. Sangeetha and U. Maitra, Supramolecular gels: Functions and uses, *Chem. Soc. Rev.*, 2005, **34**, 821–836.
4 P. Sutar and T. K. Maji, Coordination polymer gels: soft metal–organic supramolecular materials and versatile applications, *Chem. Commun.*, 2016, **52**, 8055–8074.
5 A. R. Hirst, B. Escuder, J. F. Miravet and D. K. Smith, High-Tech Applications of Self-Assembling Supramolecular Nanostructured Gel-Phase Materials: From Regenerative Medicine to Electronic Devices, *Angew. Chem., Int. Ed.*, 2008, **47**, 8002–8018.
6 S. Ray, A. K. Das and A. Banerjee, pH-Responsive, Bolaamphiphile-Based Smart Metallo-Hydrogels as Potential Dye-Adsorbing Agents, Water Purifier, and Vitamin B12 Carrier, *Chem. Mater.*, 2007, **19**, 1633–1639.
7 S. Kiyonaka, K. Sugiyasu, S. Shinkai and I. Hamachi, First Thermally Responsive Supramolecular Polymer Based on Glycosylated Amino Acid, *J. Am. Chem. Soc.*, 2002, **124**, 10954–10955.
8 S. Kobayashi, N. Hamasaki, M. Suzuki, M. Kimura, H. Shirai and K. Hanabusa, N-Alkyl Perfluoroalkanamides as Low Molecular-Mass Organogelators, *J. Am. Chem. Soc.*, 2002, **124**, 6550–6551.
9 E. D. Sone, E. R. Zubarev and S. I. Stupp, Semiconductor Nanohelices Templated by Supramolecular Ribbons, *Angew. Chem., Int. Ed.*, 2002, **41**, 1705–1709.
10 Z. Yang, G. Liang, L. Wang and B. Xu, Using a kinase/phosphatase switch to regulate a supramolecular hydrogel and forming the supramolecular hydrogel in vivo, *J. Am. Chem. Soc.*, 2006, **128**, 3038–3043.
11 A. Cayuela, S. R. Kennedy, M. L. Soriano, C. D. Jones, M. Valcárcel and J. W. Steed, Novel polymernanowires with triple hydrogen-bonding sites fabricated by metallogel template polymerization and their adsorption of thymidine, *Chem. Sci.*, 2015, **6**, 6139–6146.
12 J. B. Beck and S. J. Rowan, Multistimuli, Multiresponsive-Metallo-Supramolecular Polymers, *J. Am. Chem. Soc.*, 2003, **125**, 13922–13923.
13 D. Khatua, R. Maiti and J. Dey, A supramolecular hydrogel that responds to biologically relevant stimuli, *Chem. Commun.*, 2006, 4903–4905.
14 S. Bhattacharya and Y. Krishnan-Ghosh, First report of phase selective gelation of oil from oil/water mixtures. Possible implications toward containing oil spills, *Chem. Commun.*, 2001, 185–186.
15 L. Yao, H. Yang, Z. Chen, M. Qiu, B. Hu and X. Wang, Bismuth oxychloride-based materials for the removal of organic pollutants in wastewater, *Chemosphere*, 2021, **273**, 128576.
16 J. H. Jung, J. H. Lee, J. R. Silverman and G. John, Coordination polymer gels with important environmental and biological applications, *Chem. Soc. Rev.*, 2013, **42**, 924–936.
17 M. D. Segarra-Maset, V. J. Nebot, J. F. Miravet and B. Escuder, Control of molecular gelation by chemical stimuli, *Chem. Soc. Rev.*, 2013, **42**, 7086–7098.
18 S. Sengupta and R. Mondal, A novel gel-based approach to wastewater treatment–unique one-shot solution to potentially toxic metal and dye removal problems, *J. Mater Chem. A*, 2014, **2**, 16373–16377.
19 A. Y.-Y. Tam and V. W.-W. Yam, Recent advances in metallogels, *Chem. Soc. Rev.*, 2013, **42**, 1540–1567.
20 S. Samai and K. Biradha, Chemical and mechano responsive metal–organic gels of bis (benzimidazole)-based ligands with Cd(II) and Cu(II) halide salts: self sustainability and gas and dye, *Chem. Mater.*, 2012, **24**, 1165–1173.
21 M.-O. M. Piepenbrock, G. O. Lloyd, N. Clarke and J. W. Steed, Metal-and anion-binding supramolecular gels, *Chem. Rev.*, 2010, **110**, 1960–2004.
22 K. Murata, M. Aoki, T. Nishi, A. Ikeda and S. Shinkai, Cholesterol-based functional tectons as versatile building-blocks for liquid crystals, organic gels and monolayers, *J. Chem. Soc., Chem. Commun.*, 1991, 1715–1718.
23 S. Sengupta and R. Mondal, Elusive nanoscale metal-organic-particle-supported metallogel formation using a nonconventional chelating pyridine-pyrazole-based bis-amide ligand, *Chem. – Eur. J.*, 2013, **19**, 5537–5541.
24 M. Hao, M. Qiu, H. Yang, B. Hu and X. Wang, Recent advances on preparation and environmental applications of MOF-derived carbons in catalysis, *Sci. Total Environ.*, 2021, **760**, 143333.
25 M. Martínez-Calvo, O. Kotova, M. E. Möbius, A. P. Bell, T. McCabe, J. J. Boland and T. Gunnlaugsson, Healable luminescent self-assembly supramolecular metallogels possessing lanthanide (Eu/Tb) dependent rheological and morphological properties, *J. Am. Chem. Soc.*, 2015, **137**, 1983–1992.
26 C. K. Karan and M. Bhattacharjee, Self-Healing and Moldable Metallogels as the Recyclable Materials for Selective Dye Adsorption and Separation, *ACS Appl. Mater. Interfaces*, 2016, **8**, 5526–5535.
27 J. Liu, G. F. Gong, Y. J. Li, H. Yao, T. B. Wei and Q. Lin, Novel metallogel-based micro-acanthosphere material constructed from two tripodal gelators for efficient separation of organic dyes, *Mater. Lett.*, 2020, **274**, 128015.
28 X. Liu, H. Pang, X. Liu, Q. Li, N. Zhang, L. Mao, M. Qiu, B. Hu, H. Yang and X. Wang, Orderly Porous Covalent Organic Frameworks-based Materials: Superior Adsorbents for Pollutants Removal from Aqueous Solutions, *Innovation*, 2021, **2**, 10076.
29 X. Liu, R. Ma, L. Zhuang, B. Hu, J. Chen, X. Liu and X. Wang, Recent developments of doped g-C3N4 photocatalysts for

the degradation of organic pollutants, *Crit. Rev. Environ. Sci. Technol.*, 2021, **51**, 751–790.

30 A. Mallick, E.-M. Schön, T. Panda, K. Sreenivas, D. D. Díaz and R. Banerjee, Fine-tuning the balance between crystallization and gelation and enhancement of CO2 uptake on functionalized calcium based MOFs and metallogels, *J. Mater. Chem.*, 2012, **22**, 14951–14963.

31 K. A. Houton, K. L. Morris, L. Chen, M. Schmidtmann, J. T. A. Jones, L. C. Serpell, G. O. Lloyd and D. J. Adams, On crystal versus fiber formation in dipeptide hydrogelator systems, *Langmuir*, 2012, **28**, 9797–9806.

32 S. Saha, E.-M. Schön, C. Cativiela, D. Díaz Díaz and R. Banerjee, Proton-Conducting Supramolecular Metallogels from the Lowest Molecular Weight Assembler Ligand: A Quote for Simplicity, *Chem. – Eur. J.*, 2013, **19**, 9562–9568.

33 Y. Xu, C. Kang, Y. Chen, Z. Bian, X. Qiu, L. Gao and Q. Meng, In Situ Gel-to-Crystal Transition and Synthesis of Metal Nanoparticles Obtained by Fluorination of a Cyclic β-AminoalcoholGelator, *Chem. – Eur. J.*, 2012, **18**, 16955–16961.

34 S. Samai, P. Ghosh and K. Biradha, Does crystal or gel matter to stereochemistry of a reaction? Silver complexation-promoted solid-state [2+2] reaction of an unsymmetrical olefin, *Chem. Commun.*, 2013, **49**, 4181–4183.

35 T. Tu, W. Fang, X. Bao, X. Li and K. H. Dötz, Visual chiral recognition through enantioselective metallogel collapsing: synthesis, characterization, and application of platinum–steroid low-molecular-mass gelators, *Angew. Chem., Int. Ed.*, 2011, **50**, 6601.

36 C. Po, Z. Ke, A. Y.-Y. Tam, H.-F. Chow and V. W.-W. Yam, A Platinum(ii) Terpyridine Metallogel with an L-Valine-Modified Alkynyl Ligand: Interplay of Pt···Pt, π–π and Hydrogen-Bonding Interactions, *Chem. – Eur. J.*, 2013, **19**, 15735–15744.

37 S. Sarkar, S. Dutta, S. Chakrabarti, P. Bairi and T. Pal, Redox-Switchable Copper(i) Metallogel: A Metal–Organic Material for Selective and Naked-Eye Sensing of Picric Acid, *ACS Appl. Mater. Interfaces*, 2014, **6**, 6308–6316.

38 E. N. Zare, A. Motahari and M. Sillanpää, Nanoadsorbents based on conducting polymer nanocomposites with main focus on polyaniline and its derivatives for removal of heavy metal ions/dyes, *Environ. Res.*, 2018, **162**, 173–195.

39 G. Bjørklund, M. Dadar, J. Mutter and J. Aaseth, The toxicology of mercury: Current research and emerging trends, *Environ. Res.*, 2017, **159**, 545–554.

40 N. Sharma, P. K. Sharma, Y. Singh, C. M. Nagaraja and A. Self-Healing, Metal−Organic Gel (MOG) Exhibiting pH-Responsive Release of a Chemotherapeutic Agent, Doxorubicin: Modulation of Release Kinetics by Partial Dehydration of Matrix, *ACS Omega*, 2019, **4**, 1354–1363.

41 P. Peng, Y. Li, W. Song and X. Yu, Self-healing organogels and hydrogels constructed by self-assembled bis-terpyridine complex with selective metal ions, *Colloids Surf., A*, 2020, **589**, 124439.

42 Z. Yao, Z. Wang, Y. Yu and K. Cao, Facile synthesis and properties of the chemo-reversible and highly tunable metallogels based on polydicyclopentadiene, *Polymer*, 2017, **119**, 98–106.

43 N. Alam and D. Sarma, Facile synthesis and properties of the chemo-reversible and highly tunablemetallogels based on polydicyclopentadiene, *ACS Omega*, 2020, **5**, 17356–17366.

44 E. Saha, K. Karthick, S. Kundu and J. Mitra, Electrocatalytic Oxygen Evolution in Acidic and Alkaline Media by a Multistimuli-Responsive Cobalt(ii) Organogel, *ACS Sustainable Chem. Eng*, 2019, **7**(19), 16094–16102.

45 E. Saha and J. Mitra, Multistimuli-Responsive Self-Healable and Moldable Nickel(ii)-Based Gels for Reversible Gas Adsorption and Palladium Sequestration via Gel-to-Gel Transformation, *ACS Appl. Mater. Interfaces*, 2019, **11**(11), 10718–10728.

46 C. K. Karan and M. Bhattacharjee, Self-Healing and Moldable Metallogels as the Recyclable Materials for Selective Dye Adsorption and Separation, *ACS Appl. Mater. Interfaces*, 2016, **8**, 5526–5553.

47 A. Mishra and J. Clark, *Green Materials for Sustainable Water Remediation and Treatment*, The Royal Society of Chemistry, 2013, pp. 1–10.

48 J. W. Readman, in *An Introduction to Pollution Science*, ed. R. M. Harrison, RSC, Cambridge, 2006, pp. 77–121.

49 T. Tu, X. Bao, W. Assenmacher, H. Peterlik, J. Daniels and K. H. Dötz, Efficient Air-Stable Organometallic Low-Molecular-Mass Gelators for Ionic Liquids: Synthesis, Aggregation and Application of Pyridine-Bridged Bis(benzimidazolylidene)–Palladium Complexes, *Chem. – Eur. J.*, 2009, **15**, 1853–1861.

50 M. Roy, S. Sengupta, S. Bala, S. Bhattacharya and R. Mondal, Systematic Study of Mutually Inclusive Influences of Temperature and Substitution on the Coordination Geometry of Co(ii) in a Series of Coordination Polymers and Their Properties, *Cryst. Growth Des.*, 2016, **16**, 3170–3179.

51 R. Denoyel and E. Sabio, Rey, Solubilization in Confined Surfactant Mesophases, *Langmuir*, 1998, **14**, 7321–7323.

52 X. X. Wang, Y. N. Zhao, G. Y. Li and G. H. Cui, Self-assembly of two 2D cobalt(ii) coordination polymers constructed from 5-*tert*-butyl isophthalic acid and flexible bis(benzimidazole)-based ligand, *Transition Met. Chem.*, 2014, **39**, 653–660.

53 G. M. Sheldrick, *SHELX97*, University of Göttingen, Göttingen, Germany, 1997.